

## The Use of Microfabricated Probes to Penetrate the Internal Elastic Lamina and Intimal Hyperplasia

JAMES R. KNELLER,<sup>4</sup> CLARENCE C. WU,<sup>1</sup> DAVID A. VORP,<sup>2</sup>  
MICHAEL L. REED,<sup>5</sup> LEE E. WEISS,<sup>5</sup> HARVEY S. BOROVIETZ,<sup>4</sup>  
SIMON WATKINS,<sup>3</sup> and MARC D. FELDMAN<sup>1</sup>

### ABSTRACT

The local administration of drug or gene therapy to inhibit restenosis is currently limited by the internal elastic lamina and atherosclerotic plaque. Microprobes fabricated with micro electrical mechanical systems (MEMS) technology offers the potential for effective delivery of high concentrations of therapeutics through these barriers. However, excessive trauma in penetrating these barriers will enhance restenosis. Accordingly, we examined the importance of microprobe tip sharpness versus height in transecting the IEL and hyperplastic intima. Three groups of microprobes were examined:  $65 \pm 15$  and  $140 \pm 20$   $\mu\text{m}$  tall sharp, and  $185 \pm 25$   $\mu\text{m}$  tall blunt microprobes. Data was collected from 94 microprobes in normal and 46 microprobes in atherosclerotic rabbit iliac arteries. In normal vessels, the  $140 \pm 20$   $\mu\text{m}$  sharp microprobes all transected the IEL and did so by maintaining the transected edges adjacent to the microprobe tip minimizing vascular damage. Few  $185 \pm 25$   $\mu\text{m}$  blunt microprobes transected the IEL, but when they did, the edges were snapped well beyond the microprobe tip. All microprobes compressed the hyperplastic intima, but were not tall enough to gain entrance to the media. A novel approach to penetrate the barriers to delivery of drug and gene therapy utilizing MEMS technology is presented. Microprobe tip sharpness and associated radial stress application are more important than height. Future microprobes will have to be taller to reach the media in arteries with atherosclerosis.

### INTRODUCTION

The local administration of highly concentrated pharmacologic agents or gene therapy at the site of coronary intervention is a potential method to prevent restenosis while reducing the systemic toxicity of the infused medication.<sup>(1-3)</sup> Balloon catheters which use both passive and pressure driven diffusion, and stents have the demonstrated ability to locally deliver marker genes and pharmacologic agents into the arterial wall. However, local drug delivery has been limited by a low delivery efficiency and short intramural retention of the infused material.<sup>(4-8)</sup>

---

Departments of <sup>1</sup>Medicine, <sup>2</sup>Surgery and <sup>3</sup>Cell Biology, and Physiology, University of Pittsburgh School of Medicine.

Department of <sup>4</sup>Biomedical Engineering, University of Pittsburgh School of Engineering.

Department of <sup>5</sup>Electrical and Computer Sciences, Carnegie Mellon University.

The internal elastic lamina (IEL) inhibits the delivery of drug and gene therapy into the vessel wall. The structural ability of the IEL to prevent entry of macromolecules into the vessel has been previously demonstrated.<sup>(9-12)</sup> The IEL forms an effective barrier to substances from the size of viruses (less than 100 nm) to 10  $\mu\text{m}$  microparticles.<sup>(13,14)</sup> These findings are in agreement with Robinson et al<sup>(15)</sup> who showed that the intima of normal vessels serves as an anatomic barrier generally impermeable to microparticles in the absence of dissection. These studies support the hypothesis that transection of the IEL is necessary for the effective delivery of drugs and genes to the media.

Another barrier to the delivery of therapeutics is the atherosclerotic plaque. Feldman et al<sup>(16)</sup> delivered a reporter gene with a viral vector to both normal and atherosclerotic arteries. There was a 10-fold reduction in reporter gene transfection efficiency due to the barrier of the atherosclerotic plaque. As a result, in one of the first successful human viral transfection studies, Isner et al<sup>(17)</sup> have utilized intravascular ultrasound to identify peripheral arteries free of atherosclerosis prior to applying VEGF. Therefore both the IEL and atherosclerotic plaque remain important barriers to the delivery of therapeutics to the media and adventitia, where the biology of restenosis resides. Developing strategies to deliver drug and gene therapy through these barriers is of importance and the subject of this report.

Microfabrication is an emerging engineering technology. It enables cost effective fabrication of highly complex micro electrical mechanical systems (MEMS) using tools and batch fabrication processes developed for the integrated circuit industry. We hypothesized that microprobes developed with MEMS technology could produce controlled incisions through the IEL and atherosclerotic plaque. If successful, the potential for effective delivery of high concentration of drug or gene therapy to blood vessels would exist. Furthermore, if these microprobes were integrated on a stent, local gene and drug delivery could be administered through the plaque to the media at the time of coronary intervention to reduce restenosis.

## MATERIALS AND METHODS

### *Fabrication of microprobes*

The microprobes used in this study were fabricated via anisotropic wet etching of silicon.<sup>(18)</sup> Briefly, silicon wafers are thermally oxidized to grow a thin 1.5  $\mu\text{m}$  layer of  $\text{SiO}_2$  on the surface. The layer  $\text{SiO}_2$  is patterned using photolithography into arrays of squares. The wafers are subsequently immersed in an aqueous solution of potassium hydroxide which etches the silicon at 1.5  $\mu\text{m}/\text{min}$  but attacks the  $\text{SiO}_2$  at a reduced rate. The squares of  $\text{SiO}_2$  function as a mask which define the microprobe locations. Different planes in the silicon are etched at different rates. The four faces defining the microprobe pyramids are the fastest etching planes under the experimental conditions used. Hence, the tip shape is set by the properties of the silicon crystals. The height of the microprobes is determined by the time at which the four fast etching planes, which undercut the square  $\text{SiO}_2$  mask pattern, meet at a point.

To examine the importance of height versus microprobe tip sharpness, three groups of microprobes were examined in this study: (i)  $65 \pm 15 \mu\text{m}$  tall sharp microprobes, (ii)  $140 \pm 20 \mu\text{m}$  tall sharp microprobes, and (iii)  $185 \pm 25 \mu\text{m}$  tall blunt microprobes. The  $65 \pm 15$  and  $140 \pm 20 \mu\text{m}$  sharp microprobes had tip diameters  $\leq 3 \mu\text{m}$  and the  $185 \pm 25 \mu\text{m}$  blunt probes had square tips  $50 \pm 5 \mu\text{m}$  by  $50 \pm 5 \mu\text{m}$ . The tip-to-tip distance between the  $65 \pm 15 \mu\text{m}$  microprobes was approximately 300  $\mu\text{m}$ , and the base of each probe was approximately 40  $\mu\text{m}$  across. The tip-to-tip distance between the each  $140 \pm 20$  and  $185 \pm 25 \mu\text{m}$  microprobe was approximately 500  $\mu\text{m}$ , and the base of each microprobe was approximately 60 and 100  $\mu\text{m}$  across, respectively. Figure 1 shows scanning electron micrographs of each group. The top panel shows an individual microprobe from each group, and the lower panel at lower magnification shows the microprobe-studded wafer.

### *Rabbits and atherosclerotic model*

The iliac arteries from normal ( $n = 10$ ) and atherosclerotic ( $n = 5$ ) New Zealand white rabbits (six months to two years old, 3-4 kilograms) were used in this study. The protocol was approved by the Institutional

## PENETRATION OF IEL AND PLAQUE WITH MICROPROBES

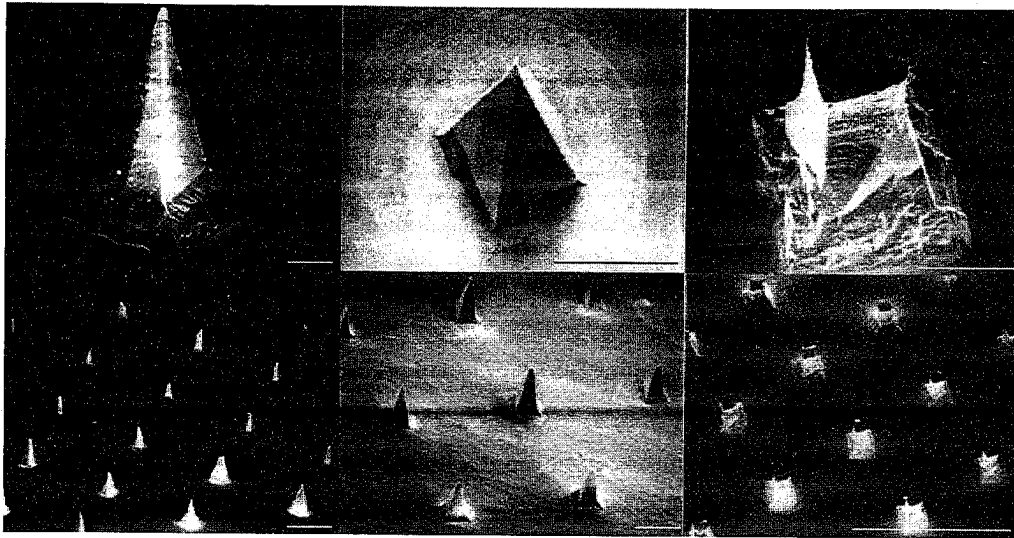


**FIG. 1.** Scanning electron micrograph of the  $65 \pm 15$  tall sharp,  $140 \pm 20$  tall sharp, and  $185 \pm 25 \mu\text{m}$  tall blunt microprobes etched on a silicon wafer in the left, middle, and right panels, respectively. A single microprobe is on the top, and a "family" of microprobes is on the bottom. Smaller bar is 10 and larger bars are  $100 \mu\text{m}$ .

Animal Care and Use Committee of the University of Pittsburgh and conformed to the National Institutes of Health Guidelines for Use of Animals in Research.

The rabbit model of atherosclerosis developed by Block et al.<sup>(19)</sup> and Faxon et al.<sup>(20)</sup> was utilized. The atherosclerotic lesions were created by feeding the rabbits a hypercholesterolemic diet containing 5% cho-

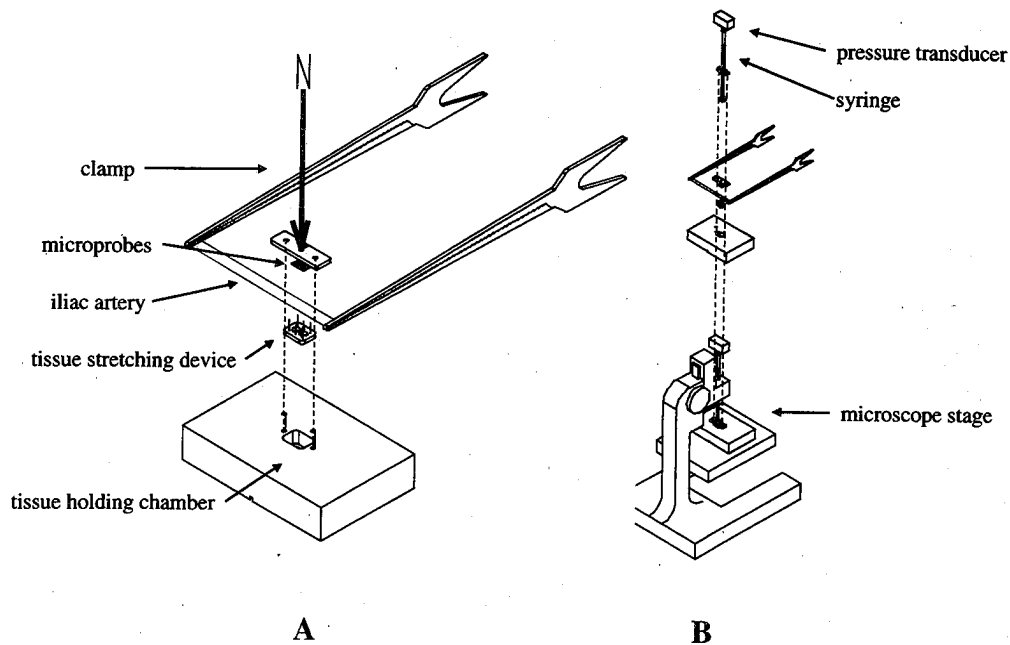


**FIG. 2.** Drawing of the customized device to hold the iliac artery at its *in situ* length, apply the microprobes to the endothelial surface at a measurable pressure, and preserve the microprobe-tissue interaction for latter microscopic examination. A. A close-up of the iliac artery and microprobes. B places 2A on the apparatus to apply and measure pressure times area of the silicon wafer or N. See text for further detail.

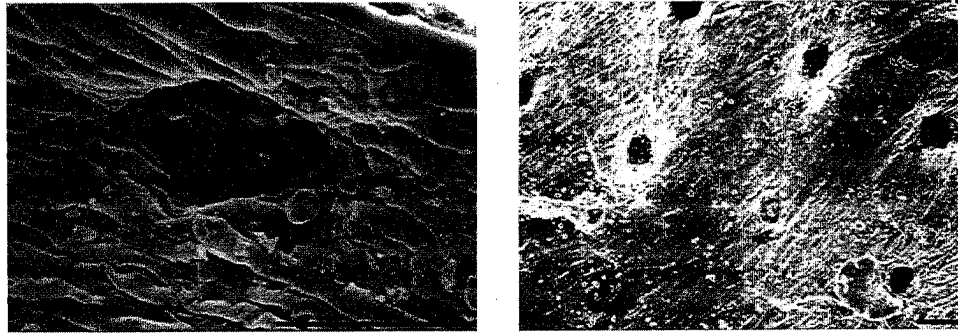


FIG. 3. Scanning electron micrograph of a typical single microprobe incision (left) and "family" of incisions (right) of a normal rabbit iliac artery with preservation of the surrounding endothelial surface. The bars represent 100  $\mu\text{m}$ .

lesterol and 7% peanut oil for a period of three weeks. Arterial balloon injury to the iliac artery was then performed with a 2F Fogarty catheter and the hypercholesterolemic diet was resumed for another 3–5 weeks.

#### Pressure range examined

Since the microprobes are to be deployed from an intravascular stent, clinical conditions were simulated. Stent deployment in patients results in 10 to 30% circumferential vessel distention. The intraluminal pressures corresponding to these amounts of distention may be determined from previous compliance measurements of normal and atherosclerotic rabbit arteries.<sup>(21)</sup> The intraluminal pressure range ( $\Delta P$ ) needed to distend the artery during stenting is related to its compliance ( $C$ ) and volume change ( $\Delta V$ ) of the vessel by equation (1)

$$\Delta P = \Delta V/C \quad (1)$$

For normal and atherosclerotic rabbit vessels, the compliance values were reported to be  $0.058 \times 10^{-3}$  and  $0.061 \times 10^{-3}$  ml/mm Hg, respectively.<sup>(21)</sup> Assuming a unit length of vessel and a concentric atherosclerotic lesion and using the mean diameter of rabbit iliac arteries previously determined,<sup>(22)</sup> these compliance values correspond to intraluminal pressures ranging from 143 to 500 mm Hg (see Appendix A). Based on these calculations, pressures of 100, 300, and 500 mm Hg were selected for this study. The same application pressures were used for normal and atherosclerotic vessels because the calculated pressure ranges were similar.

#### Protocol

To harvest the iliac arteries, rabbits were sedated with 5 mg/kg sq xylazine (Miles, Shawnee Mission, KA) and 0.1 mg/kg atropine (Liphomed, Deerfield, IL) followed by general anesthesia with 40 mg/kg iv ketamine (Fort Dodge Lab., Fort Dodge IA) and 0.1 mg/kg acepromazine (Aveco, Fort Dodge, IA). The

TABLE 1. INCIDENCE OF IEL TRANSECTION IN NORMAL VESSELS

Microprobe Group ( $\mu\text{m}$ )	Pressure (mm Hg)		
	100	300	500
Sharp $65 \pm 15$	0/10	0/8	0/16
Sharp $140 \pm 20$	7/7	7/7	10/10
Blunt $185 \pm 25$	1/11	1/10	0/15

$n^1/n^2$  where  $n^1$  = number of occurrences,  $n^2$  = number of microprobes observed.

## PENETRATION OF IEL AND PLAQUE WITH MICROPROBES

tissue handling protocol developed by Fry et al. for filleted arteries *in vitro* was followed.<sup>(23-25)</sup> Both iliac arteries were dissected from the distal side of the inguinal ligament to the abdominal wall. The base of the aorta was ligated to allow cannulation of the iliac branch, permitting pressure perfusion with medium to rinse the vessel free of blood. The vessel was opened longitudinally along its dorsal aspect, and clamped (Figure 2A) as a planar sheet at its *in situ* length according to the methods of Brant et al.<sup>(26)</sup> to maintain a confluent endothelial monolayer. Following excision, the vessel was bathed in Cellgro™ 199 *in vitro* Cell Culture medium (Mediatech®) at 37°C.

Harvested segments were mounted, endothelial side up, on a customized tissue holding device (Figure 2A). The *in situ* circumference of the artery was then restored by a 1.4 fold distension with a tissue stretching device.<sup>(27)</sup> The arteries final circumferential dimensions ranged from 0.795 to 0.939 cm (see Appendix B). The microprobes, iliac artery, and the tissue stretching device were all lowered into a tissue holding chamber. The microprobes were then applied to the vessel lumen and pressure applied (N, see Figures 2A and B) via a microscope stage. Pressure was monitored via an inverted syringe attached to a fluid filled transducer. During pressure application, the media was removed and replaced with 2.5% glutaraldehyde in phosphate buffer for 20 min. to preserve the microprobe-tissue interactions. The microprobes were removed and the tissue fixed for an additional 60 min.

### *Tissue processing and imaging*

Transmitted electron microscope (TEM) was utilized to examine mechanisms of IEL failure but not for the incidence of IEL and EEL transection due to the large number of sections required. The distances between the microprobes, and the 60 nm sections cut for TEM imply that every 80 of 5,000 to 8,000 ultra microtome sections examined will reveal the tip of a sharp microprobe, and every 800 of the 8,000 ultra microtome sections will reveal the tip of a blunt microprobe.

Tissues were stained with 1% osmium tetroxide for 1 hr at 4°C. Dehydration was performed with ethanol rinses. The tissue was saturated with Epon, then cured at 60°C for 24 hrs. 60 nm sections were cut with an ultra microtome (Sorvall MT 500), and imaged with TEM (Jeol JEM-100CXII).

Scanning electron microscopy was used to evaluate microprobe interaction with the endothelial surface. Tissues were dehydrated using the TEM protocol, then pinned to wax wafers. The samples were dried in a thermoelectric critical point dryer (Emscope CPD 750) and placed in a specimen chamber with 100% ethanol. A series of soaking and venting steps with CO<sub>2</sub> were performed until no ethanol could be detected. The chamber temperature was raised from 10 to 40°C to dry the specimens. Dried tissue was sputter coated with



**FIG. 5.** A transmitted electron micrograph showing an alternative mechanism of IEL transection for the  $185 \pm 25$   $\mu\text{m}$  tall blunt microprobe in a normal iliac artery. The IEL (thick gray structure) has torn off to the side of the tissue indentation from the microprobe. Bar is 10  $\mu\text{m}$ .

TABLE 2. INCIDENCE OF EEL TRANSECTION IN NORMAL VESSELS

Microprobe Group ( $\mu\text{m}$ )	Pressure (mm Hg)		
	100	300	500
Sharp $65 \pm 15$	0/10	0/8	0/16
Sharp $140 \pm 20$	0/7	0/7	2/10
Blunt $185 \pm 25$	0/11	0/10	0/15

$n^1/n^2$  where  $n^1$  = number of occurrences,  $n^2$  = number of microprobes observed.

gold and palladium (Technics Hummer VI), and placed on aluminum mounting platforms. Samples were then placed in the sample chamber and imaged (Jeol JSM-T300).

Light superimposed with fluorescence microscopy was used to quantitate IEL and EEL transection and plaque compression by the microprobes. Six  $\mu\text{m}$  sections of tissue were cryosectioned (Microm HM 505 E) with approximately 200–250 sections collected per sample. The distances between microprobes imply that 50 to 80 cryosections must be collected for each  $65 \pm 15 \mu\text{m}$ , and  $140 \pm 20$  or  $185 \pm 25 \mu\text{m}$  microprobe group, respectively. Since this is less time intensive than using electron microscopy, light microscopy was chosen as the principle means to quantitate tissue—microprobe interactions.

Samples were transferred from the fixative to 30% sucrose for 24 hrs, then frozen in isopentane chilled in liquid nitrogen. Following sectioning, normal iliac arteries were stained with hematoxylin and eosin. Atherosclerotic iliac arteries were stained with Oil red O-isopropanol with hematoxylin as a counterstain. Both vessel types were imaged with a light microscope (Olympus Provis AX70). A fluorescence microscope was used to autofluoresce the IEL and EEL. The fluorescence image was superimposed on the light field image to determine if the IEL and EEL had been transected. Transection was defined as cell nuclei which are at 90 degrees to the adjacent microprobe tip. Compression, in contrast, was defined as cell nuclei which run parallel to the adjacent microprobe tip.

## RESULTS

### Normal rabbit iliac arteries

The microprobes produced precise incisions into the intima of the normal iliac arteries. Figure 3 demonstrates a SEM showing both a “family” of microprobe incisions and a typical single microprobe incision at higher magnification. The endothelial cells are only disrupted at the exact site of microprobe contact, with no damage to the surrounding endothelium.

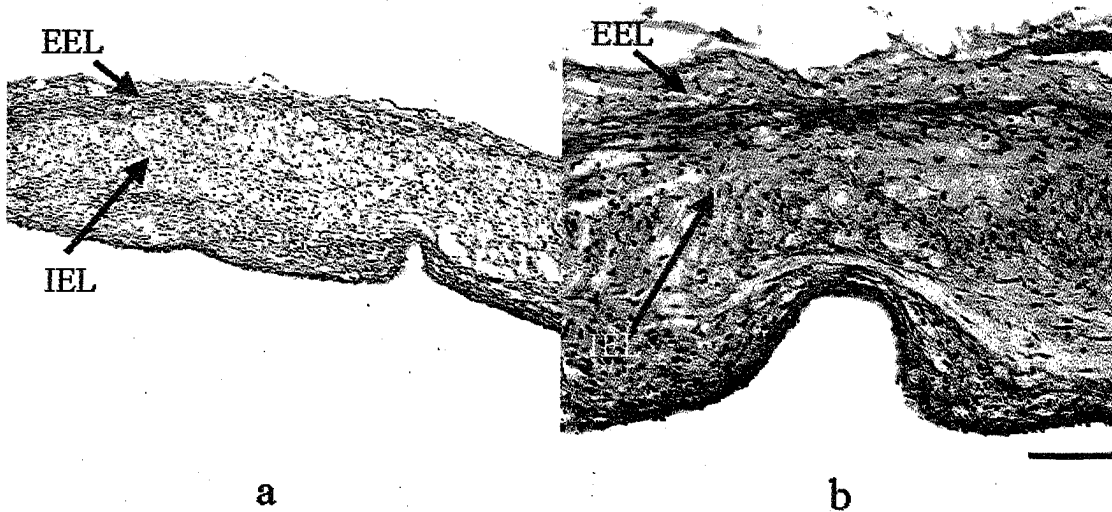
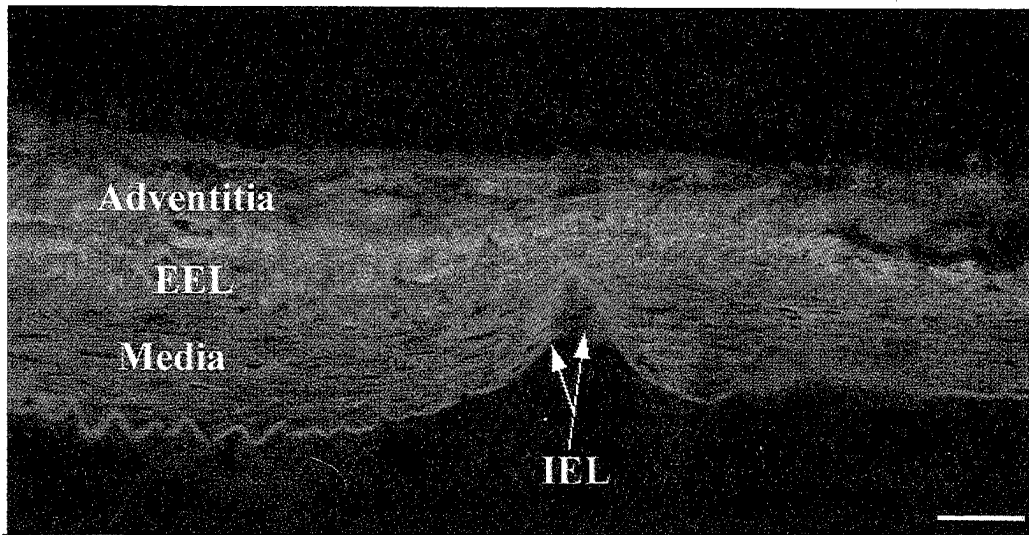
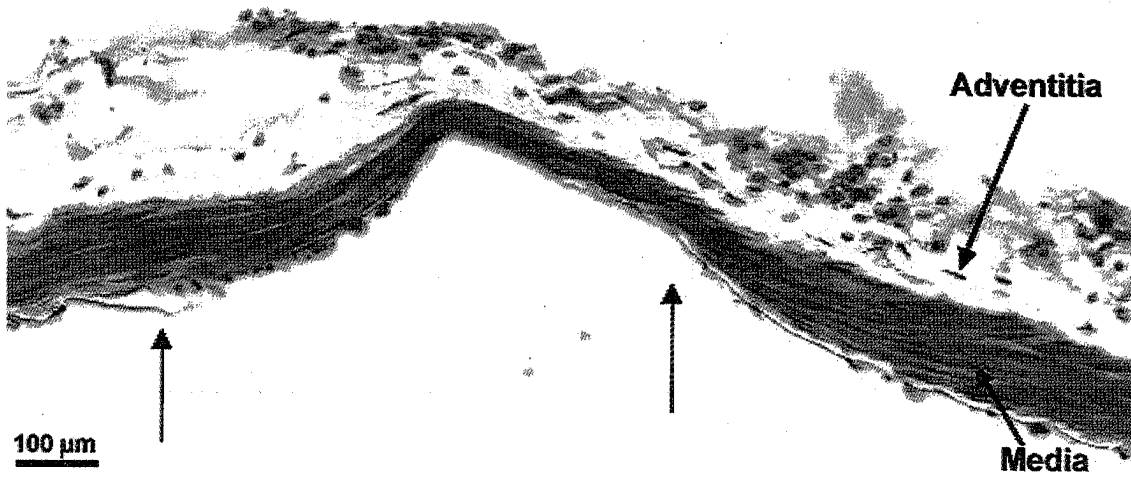
Data were collected from 94 microprobes in normal rabbit iliac arteries. The incidence of IEL transection for the 3 types of microprobes at the 3 pressures examined is summarized in Table 1. The  $65 \pm 15 \mu\text{m}$

**FIG. 4.** The mechanism of IEL transection with the  $185 \pm 25 \mu\text{m}$  tall blunt microprobes in a normal iliac artery is shown. The edges of the cut IEL (arrows) are snapped well beyond the vessel indentation from the microprobe.

**FIG. 6.** The mechanism of IEL transection with the  $140 \pm 20 \mu\text{m}$  tall sharp microprobe in an iliac artery is shown (45). A light superimposed with a fluorescence microscope image demonstrates that the ends of the transected IEL (arrows) remain adjacent to the microprobe plane of transection due to piercing. Bar is  $100 \mu\text{m}$ .

**FIG. 8.** A light superimposed with a fluorescence microscope image is used to show examples of plaque compression from a  $140 \pm 20 \mu\text{m}$  tall sharp microprobe (A) and a  $185 \pm 25 \mu\text{m}$  tall blunt microprobe (B) in atherosclerotic rabbit iliac arteries. The microprobes used in this study were not tall enough to penetrate through the plaque to the media. Bar is  $100 \mu\text{m}$  for the right panel, and  $200 \mu\text{m}$  for the left panel.

PENETRATION OF IEL AND PLAQUE WITH MICROPROBES



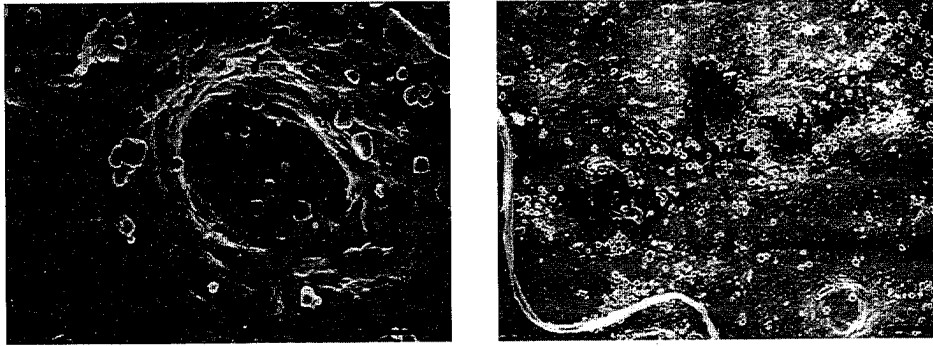


FIG. 7. Scanning electron micrograph of a typical single microprobe incision (left) and "family" of 4 incisions (right) in an atherosclerotic rabbit iliac artery. Disruption of the plaque is only at the site of microprobe contact. Bars are 100  $\mu\text{m}$ .

sharp microprobes compressed the IEL and failed to transect into the media for all 34 examined at 100, 300, and 500 mm Hg applied pressure. The  $140 \pm 20 \mu\text{m}$  sharp microprobes, however, transected the IEL for all 24 examined at every pressure examined. Despite being taller, the  $185 \pm 25 \mu\text{m}$  blunt microprobes compressed the IEL without transecting it in 34 of 36 examined. The two IEL transections occurred at the lower applied pressures of 100 and 300 mm Hg, but not at 500 mm Hg.

The mechanism of IEL transection was examined. The 2 of 36  $185 \pm 25 \mu\text{m}$  blunt microprobes which did transect the IEL did so via tearing as opposed to piercing, snapping the incision points of the IEL beyond the  $50 \pm 5 \mu\text{m}$  surface size of these microprobes (Figure 4). A TEM shows alternative mechanisms of IEL disruption caused by the  $185 \pm 25 \mu\text{m}$  blunt microprobes (Figure 5). The transection of the IE is not at the point of contact of the blunt microprobe to the vessel, but rather off to the side. In contrast to these tears, the mechanism of IEL transection by the  $140 \pm 20 \mu\text{m}$  sharp microprobes was via piercing. Accordingly, the ends of the transected IEL remained adjacent to the microprobe plane of transection. An example of this pattern is shown in Figure 6.

The incidence of EEL transection was also quantitated for the 3 types of microprobes at the 3 pressures examined and is shown in Table 2. Neither the  $65 \pm 15 \mu\text{m}$  sharp nor the  $185 \pm 25 \mu\text{m}$  blunt microprobes transected the EEL at any pressure with data from 70 microprobes. However, 2 of 24  $140 \pm 20 \mu\text{m}$  sharp microprobes did transect the EEL but only at the 500 mm Hg pressure.

#### *Atherosclerotic rabbit iliac arteries*

The taller microprobes produced precise incisions into the hyperplastic intima. Figure 7 demonstrates a SEM showing both a "family" of microprobe incisions and a typical single microprobe incision at higher magnification. The disruption of the plaque is only at the site of microprobe contact.

TABLE 3. INCIDENCE OF PLAQUE COMPRESSION IN ATHEROSCLEROTIC VESSELS

Microprobe Group ( $\mu\text{m}$ )	Pressure (mm Hg)		
	100	300	500
$140 \pm 20$ sharp	7/7	5/5	8/8
$185 \pm 25$ blunt	9/9	10/10	7/7

$n^1/n^2$  where  $n^1$  = number of occurrences,  $n^2$  = number of microprobes observed.

## PENETRATION OF IEL AND PLAQUE WITH MICROPROBES

TABLE 4. INCIDENCE OF IEL TRANSECTION  
IN ATHEROSCLEROTIC VESSELS

<i>Microprobe</i>	<i>Pressure (mm Hg)</i>		
<i>Group (<math>\mu\text{m}</math>)</i>	<i>100</i>	<i>300</i>	<i>500</i>
140 $\pm$ 20 sharp	0/7	0/5	1/8
185 $\pm$ 25 blunt	0/9	0/10	0/7

$n^1/n^2$  where  $n^1$  = number of occurrences,  $n^2$  = number of microprobes observed.

Data were collected from 46 microprobes in atherosclerotic rabbit iliac arteries. Since the  $65 \pm 15 \mu\text{m}$  microprobes did not transect the IEL of normal arteries, they were not examined. The incidence of plaque compression was quantitated for the 2 taller microprobes at the 3 pressures examined and is shown in Table 3. The  $140 \pm 20 \mu\text{m}$  sharp microprobes compressed the plaque for all 20 examined at all 3 pressures applied. The incidence of IEL transection, however, was only 1 of 20 examined and only at 500 mm Hg as shown on Table 4. The  $185 \pm 25 \mu\text{m}$  blunt microprobes compressed the plaque for all 26 examined at all 3 pressures applied. There were no instances of IEL transection as shown on Table 4. There were also no instances of EEL transection for both of these taller microprobes. Examples of these are shown in Figure 8 and demonstrate that the microprobes used in these studies were not tall enough to penetrate through the plaque to the media.

### DISCUSSION

This study has demonstrated that microprobes developed with microelectrical mechanical systems (MEMS) technology could produce controlled incisions to the major barriers to local drug and gene therapy, the internal elastic lamina and intimal hyperplasia used as a surrogate for atherosclerotic plaque. For normal rabbit iliac arteries, the  $65 \pm 15 \mu\text{m}$  sharp microprobes compressed but were too short to transect the IEL. The  $140 \pm 20 \mu\text{m}$  sharp microprobes consistently transected the IEL and gained entrance to the media. They did so by maintaining the ends of the transected IEL adjacent to the microprobe tip of  $3 \pm 2 \mu\text{m}$  and thereby minimizing vascular damage. The  $185 \pm 25 \mu\text{m}$  blunt microprobes, however, rarely transected the IEL despite being taller. When they did transect the IEL, the ends of the IEL were snapped beyond the  $50 \pm 5$  by  $50 \pm 5 \mu\text{m}$  tip. Applied force was relevant for transection of the EEL. The  $140 \pm 20 \mu\text{m}$  sharp microprobes penetrated into the adventitia only at 500 mm Hg. Finally, the taller microprobes consistently compressed the intimal hyperplasia. However, they were rarely tall enough to transect the IEL and gain entrance into the media.

The differences in how the 140 and 185  $\mu\text{m}$  microprobes cut the IEL (*i.e.*, piercing versus tearing, respectively) are in keeping with biomechanical aspects of probe height and tip size. The taller microprobes will generate greater circumferential strain applied to the arterial wall and the IEL. Circumferential strain is given by the ratio of the distorted fiber length to the original, unstrained length. Since circumferential strain gives rise to circumferential stress, the taller the microprobe, the greater the circumferential stress placed on the IEL. Next, consider the implications of microprobe sharpness. The sharper the microprobe tip, the smaller the area of contact of the probe tip with the arterial wall and IEL. The total force  $F$  transmitted through the MEMS silicon wafer to the arterial wall is given by:

$$F = \sum \sigma_r \times A \quad (2)$$

where  $\sigma_r$  is the radial stress developed at each microprobe tip and  $A$  is the surface area of each tip. If it is assumed that the tip shape of all the microprobes on the wafer are identical and circular, then  $A = \pi R^2$

where  $R$  is the tip radius. If it is assumed that the force is evenly distributed between the probes, then

$$\sigma_r = F/(N\pi R^2) \quad (3)$$

where  $N$  is the total number of microprobes on the wafer. Equation 3 illustrates the importance of tip sharpness on radial stress. The sharper the tip, the smaller its radius  $R$ , and the greater the radial stress. The above logic indicates that the microprobe height has the greatest influence on applied circumferential stress, whereas microprobe sharpness has the greatest influence on radial stress. When applied to mechanisms of IEL transection, elevated circumferential stress would promote tearing of the IEL whereas elevated radial stress would promote piercing. These predictions are consistent with our observations that the blunt 185  $\mu\text{m}$  microprobe caused a larger IEL transection consistent with tearing (see Figures 4 and 5). The sharp 140  $\mu\text{m}$  microprobe caused a more focal IEL transection consistent with piercing (see Figure 6).

These observations are relevant because excessive trauma in penetrating these barriers can enhance the development of atherosclerosis and restenosis. Sims and coworkers<sup>(10,28-29)</sup> demonstrated that the difference in incidence in arteriosclerosis between coronary and internal mammary arteries is related to the integrity of the IEL. In autopsy specimens from 300 patients, they demonstrated that the mammary artery showed only minimal defects in the IEL at all ages while the coronary arteries showed substantial defects in the IEL which increased with age. Furthermore, the defects in the IEL were associated with the presence of medial cells in the intima, and the thickness of the intima correlated with the magnitude of the defects in the IEL. The implication is that greater separation of the IEL by the 185  $\mu\text{m}$  microprobes due to circumferential stress may accelerate the progression of arteriosclerosis.

The magnitude of the IEL fracture also correlates with the extent of intimal hyperplasia in coronary restenosis. Schwartz and coworkers<sup>(30-31)</sup> have demonstrated that the structural integrity of the IEL is critical to minimize intimal hyperplasia. In their studies, the mean intimal thickness increased as a mean injury score which reflected laceration of the internal elastic lamina increased. They also present evidence that the intimal proliferative response at each IEL break is proportional to the size of the break. Morimoto et al.<sup>(32)</sup> made similar observations in human restenosis. The implication is the greater separation of the IEL by the 185  $\mu\text{m}$  microprobes due to circumferential stress may magnify the amount of intimal hyperplasia. Any future stent studded with microprobes will require sharp tips to minimize the extent of damage to the IEL.

Biological applications of engineering devices developed with microelectrical mechanical systems (MEMS) is in an early stage. Most of these applications are in diagnostics; *i.e.*, microfabricated pressure transducers<sup>(33)</sup> and microforce sensors.<sup>(34)</sup> Other applications include microfabricated sample injectors and liquid dosing systems,<sup>(35-36)</sup> microsystems for measurement and dosage of volatile anesthetics,<sup>(37)</sup> and intraocular lens delivery devices and retina implants.<sup>(38)</sup> More recently, there has been considerable intent in so-called "lab-on-a-chip" applications where a large number of chemical or biological assays are performed in parallel including microminiaturization of molecular genetic analysis and cell free protein synthesis.<sup>(39)</sup> In an application similar to ours, Henry et al.<sup>(40)</sup> micromachined needles for the transdermal delivery of drugs. They demonstrated four orders of magnitude enhanced skin permeability to a drug with the application of micro-needles. Similarly, the goal of the microprobes is to enhance the delivery of drug or gene therapy through atherosclerotic plaque. The long term plan is to fabricate a stent with integrated microprobes to produce controlled incisions through plaque, enabling the delivery of high concentrations of drug or gene therapy during and after coronary intervention to regulate intimal hyperplasia, thereby minimizing restenosis.

There are several limitations to this study. Important differences exist between human atherosclerosis and the rabbit model of neointimal hyperplasia. The stiffness of mature human plaque exceeds that of the rabbit model used in this study. This arises from the absence of calcification and fibrosis in the rabbit model. Loree et al.<sup>(41)</sup> divided human plaques into three groups, cellular, hypocellular, and calcified. The reported circumferential tangential stiffness moduli of these plaques were  $927 \pm 468$  kPa,  $2312 \pm 2180$  kPa, and  $1466 \pm 1284$  kPa, respectively. A similar range was reported by Lendon et al.<sup>(42)</sup> Based on these figures, the intraluminal pressure needed to distend a concentric lesion by 30% ranges from 1209 to 3016 mmHg for these 3 types of human plaque. Consequently, the intraluminal pressures used to simulate stenting in this study are lower than those which would be required for human atherosclerosis by a factor of 2.4 to 6.0.

The applied force in the current study is underestimated, however, due to the technology utilized. The

## PENETRATION OF IEL AND PLAQUE WITH MICROPROBES

MEMS structures tested were fabricated on planar silicon wafers. The base of the wafer prevents the microprobes from penetrating beyond their height. Cylindrical stents are a mesh which allows the stent itself to be embedded into the vessel wall. Microprobes incorporated onto a stent will therefore deliver a greater applied force to the vessel for a given pressure applied to the base of the microprobes. The ability to etch a microprobe on a curved surface was recently demonstrated and makes the manufacture of a stent with incorporated microprobes feasible.<sup>(43)</sup>

Finally, human plaques are often eccentric with irregular surfaces. The implication is that microprobes of constant height on a stent would not all have access to the media. However, a recent study by Mintz and coworkers<sup>(44)</sup> demonstrated that one mechanism of balloon angioplasty increasing coronary artery lumen size is via axial redistribution of plaque to more even proportions. Furthermore, microprobe studded stents could have microprobes of varying heights manufactured.

In conclusion, a novel approach to penetrate the major barrier of delivery of therapeutics to the media and adventitia has been presented. The importance of microprobe tip sharpness and radial stress application to minimize the degree of IEL transection is also demonstrated. Future microprobes of greater height will need to be fabricated to penetrate atherosclerotic plaque.

### ACKNOWLEDGMENTS

This work was in part supported by a FIRST Award (R29-H247046-01) (MDF). The work was presented in abstract form in part at the American College of Cardiology 47th Scientific Session, 1998. Important contributions were made by J.E.B. Burchenal, William R. Wagner, and James F. Antaki.

### REFERENCES

1. Wolinsky H, Thung SN. Use of a perforated balloon catheter to deliver concentrated heparin into the wall of the normal canine artery. *J Am Coll Cardiol* 1990;15:475-481.
2. Nabel EG, Plautz G, Nabel GJ. Site specific gene expression in vivo by direct gene transfer into the arterial wall. *Science* 1990;244:1285-1288.
3. Hofling B, Huehns TY. Intravascular local drug delivery and angioplasty. *Eu Heart J* 1995;16:437-440.
4. Lambert TL, Vishva D, Rechavia E, Forrester JS, Litvack F, Eigler NL. Localized arterial drug delivery from a polymer coated removable metallic stent. *Circulation* 1994;90:1003-1011.
5. Gradus-Pizlo I, Wilensky RL, March KL, Sandusky GE, Fineberg NS, Michaels M, Hathaway DR. Local delivery of biodegradable microparticles containing colchicine or a colchicine analog: Effects on restenosis and implications for catheter based drug delivery. *J Am Coll Cardiol* 1995;26:1549-1557.
6. Azrin MA, Mitchel JF, Fram DB, Pedersen CA, Cartun RW, Barry JJ, Bow LM, Waters DD, McKay RG. Decreased platelet deposition and smooth muscle cell proliferation after intramural heparin delivery with hydrogel coated balloons. *Circulation* 1994;90:433-441.
7. Wilensky RL, March KL, Hathaway DR. Direct intra-arterial wall injection of microparticles via a catheter: A potential drug delivery strategy following angioplasty. *Am Heart J* 1991;122:1136-1140.
8. Wilensky RL, March KL, Gradus-Pizlo I, Schauwecker D, Michaels M, Robinson J, Carlson K, Hathaway DR. Regional and arterial localization of radioactive microparticles after local delivery by unsupported or supported porous balloon catheters. *Am Heart J* 1995;129:852-859.
9. Penn MS, Rangaswamy S, Sidel GM, Chisolm GM. Macromolecular transport in the arterial intima: Comparison of chronic and acute injuries. *Am J Physiol* 1997;272 (Heart Circ Physiol 41):H1560-H1570.
10. Sims FH. The internal elastic lamina in normal and abnormal human arteries: a barrier to the diffusion of macromolecules from the lumen. *Artery* 1989;16:159-173.
11. Smith EB, Staples EM. Distribution of plasma proteins across the human aortic wall: barrier functions of endothelium and internal elastic lamina. *Atherosclerosis* 1980;37:579-590.

12. Smith EB. Transport, interactions and retention of plasma proteins in the intima: the barrier function of the internal elastic lamina. *Eur Heart J* 1990;11(suppl E):72-81.
13. Nasser TK, Wilensky RL, Khawar M, March KL. Microparticle deposition in periarterial microvasculature and intramural dissections after porous balloon delivery into atherosclerotic vessels: quantitation and localization by confocal scanning laser microscopy. *Am Heart J* 1996;131:892-898.
14. Rome JJ, Shayani V, Flugelman MY, Newman KD, Farb A, Virmani R, Dichek DA. Anatomic barriers influence the distribution of in vivo gene transfer into the arterial wall: modeling with microscopic tracer particles and verification with a recombinant adenoviral vector. *Arterioscler Thomb* 1994;14:148-161.
15. Robinson KA, Waksman R, Chronos N, Cipolla GD, Sigman SR, Thomas CN, King SB. Focal delivery of microparticles to sites of balloon angioplasty in pig coronary arteries: Acute deposition and chronic retention patterns. *Circulation* 1994;90:I-19 (abstract).
16. Feldman LJ, Steg PG, Zheng LP, Chen D, Kearney M, McGarr SE, Barry JJ, Dedieu JF, Perricaudet M, Isner JM. Low efficiency of percutaneous adenovirus mediated arterial gene transfer in the atherosclerotic rabbit. *J Clin Invest* 1995;95:2662-2671.
17. Isner JM, Pieczek A, Schainfeld R, Blair R, Haley L, Asahara T, Rosenfield K, Razvi S, Walsh K, Symes JF. Clinical evidence of angiogenesis after arterial gene transfer of phVEGF<sub>165</sub> in patient with ischaemic limb. *Lancet* 1996;348:370-374.
18. Han H, Weiss LE, Reed ML. Micromechanical velcro. *IEEE J Microelectromechanical systems* 1992;1(1):37-43.
19. Block PC, Gaughman KL, Pasternak RC, Fallon JT. Transluminal angioplasty: correlation of morphologic and angiographic findings in an experimental model. *Circulation* 1980;61:778-785.
20. Faxon DP, Sanborn TA, Weber VJ, Haudenschild C, Gottsman SB, McGovern WA, Ryan TJ. Restenosis following transluminal angioplasty in experimental atherosclerosis. *Arteriosclerosis* 1984;4:189-195.
21. Zuckerman BD, Weisman HF, Yin FCP. Arterial hemodynamics in a rabbit model of atherosclerosis. *Am J Physiol* 1989;257:H891-897.
22. Berceli S. Hemodynamics and atherogenesis: low density lipoprotein metabolism and endothelial cell morphology. Ph.D. dissertation 1990, School of Engineering, University of Pittsburgh.
23. Fry DL. Aortic evans blue dye accumulation: its measurement and interpretation. *Am J Physiol* 1977;232(2):H204-H222.
24. Fry DL, Mahley RW, Suk YO. Effect of arterial stretch on transmural albumin and evans blue dye transport. *Am J Physiol* 1981;240:H645-H649.
25. Fry DL, Mahley RW, Weisgraber KH, Suk YO. Simultaneous accumulation of evans blue dye and albumin in the canine aortic wall. *Am J Physiol* 1977;233(1):H66-H79.
26. Brant A. Hemodynamics and mass transfer aspects of arterial disease. Ph.D. dissertation 1986, School of Engineering, University of Pittsburgh.
27. Fry DL, Cornhill FJ, Sharma H, Pap JM, Mitschelen J. Uptake of low density lipoprotein, albumin, and water by de-endothelialized in vitro minipig aorta. *Arteriosclerosis* 1986;6:475-490.
28. Sims FH. Discontinuities in the internal elastic lamina: a comparison of coronary and internal mammary arteries. *Artery* 1985;13(3):127-143.
29. Sims FH, Gavin JB, Vanderwee MA. The intima of human coronary arteries. *Am Heart J* 1989;118:32-38.
30. Schwartz RS, Huber KC, Murphy JG, Edwards WD, Camrud AR, Vlietstra RE, Holmes DR. Restenosis and the proportional neointimal response to coronary artery injury: results in a porcine model. *J Am Coll Cardiol* 1992;19:267-274.
31. Schwartz RS, Murphy JG, Edwards WD, Camrud AR, Vlietstra MB, Holmes DR. Restenosis after balloon angioplasty: a practical proliferative model in porcine coronary arteries. *Circulation* 1990;82:2190-2200.
32. Morimoto S, Mizuno Y, Hiramitsu, et al. Restenosis after percutaneous transluminal coronary angioplasty: histopathological study using autopsied hearts. *Jpn Circ J* 1990;54:43-56.
33. Kalvesten E, Smith L, Tenez L, Stemme G. The first surface micromachined pressure sensor for cardiovascular pressure measurements. *IEEE Proceedings, 11th annual international workshop, Micro Electro Mechanical Systems* 1998;574-579.

## PENETRATION OF IEL AND PLAQUE WITH MICROPROBES

34. Tanimoto M, Arai F, Fukuda T, Iwata H, Itoigawa K, Gotoh Y, Hasimoto M, Negoro M. Micro force sensor for intravascular neurosurgery and in vivo experiment. IEEE Proceedings, 11th annual international workshop, Micro Electro Mechanical Systems 1998;504-509.
35. Man PF, Mastrangelo CH, Burns MA, Burke DT. Microfabricated capillarity driven stop valve and sample injector. IEEE Proceedings, 11th annual international workshop, Micro Electro Mechanical Systems 1998;45-50.
36. Roberg R, Sandmaier H. Portable micro liquid dosing system. IEEE Proceedings, 11th annual international workshop, Micro Electro Mechanical Systems 1998;526-531.
37. Burte EP, Rintelmann K, Temmel G. Microsystems for measurement of dosage of volatile anesthetics and respiratory gases in anesthetic equipment. IEEE Proceedings, 11th annual international workshop, Micro Electro Mechanical Systems 1998;510-514.
38. Trieu HK, Ewe L, Mokwa W, Schwarz M, Hosticka BJ. Flexible silicon structures for a retina implant. IEEE Proceedings, 11th annual international workshop, Micro Electro Mechanical Systems 1998;515-519.
39. Koji I, Maruo S, Fukaya Y, Fujisawa T. Biochemical ic chip toward cell free DNA protein synthesis. IEEE Proceedings, 11th annual international workshop, Micro Electro Mechanical Systems 1998;131-136.
40. Henry S, McAllister DV, Allen MG, Prausnitz MR. Micromachined needles for the transdermal delivery of drugs. IEEE Proceedings, 11th annual international workshop, Micro Electro Mechanical Systems 1998;494-498.
41. Loree HM, Grodzinsky AJ, Park SY, Gibson LJ, Lee RT. Static circumferential tangential modulus of human atherosclerotic tissue. J Biomechanics 1994;27(2):195-204.
42. Lendon CL, Briggs AD, Born G, Burleigh MC, Davies MJ. Mechanical testing of connective tissue in the search for determinants of atherosclerotic plaque cap rupture. Biochem Soc Trans 1988;16(2):1032-1033.
43. Nadeem A, Mescher M, Rebello K, Weiss LE, Wu C, Feldman MD, Reed ML. Fabrication of microstructures using aluminum anodization techniques. IEEE Proceedings, 11th annual international workshop, Micro Electro Mechanical Systems 1998;274-277.
44. Mintz GS, Pichard AD, Kent KM, Satler LF, Popma JJ, Leon MB. Axial plaque redistribution as a mechanism of percutaneous transluminal coronary angioplasty. Am J Cardiol 1996;77:427-430.
45. Reed ML, Wu C, Kneller J, Watkins S, Vorp DA, Nadeem A, Weiss LE, Rebello K, Mescher M, Smith AJ, Rosenblum W, Feldman MD. Micromechanical devices for intravascular drug delivery. J Pharm Sci 1998;87:1387-1394.

Address reprint requests to:

*Marc D. Feldman, M.D.*

*Room 5.642U, Division of Cardiology*

*University of Texas Health Science Center at San Antonio*

*7703 Floyd Curl Drive*

*San Antonio, Texas 78284-7872*

## APPENDIX A

Pressure calculations for rabbit iliac arteries. Zukerman et al.<sup>(21)</sup> measured the compliance of atherosclerotic rabbit iliac arteries at 10 and 30% distention. Berceci<sup>(22)</sup> measured the internal diameter of the proximal and distal rabbit iliac artery. From these measurements, the compliance values can be used to determine the intraluminal pressure needed to achieve this degree of arterial distension. These values were chosen to simulate stented coronary arteries.

Proximal internal diameter: 0.26 cm

Distal internal diameter: 0.20 cm

Mean internal radius ( $r_0$ ): 0.115 cm

Mean internal radius with 10% distension ( $r_{10}$ ):  $0.115 + 0.115(0.10) = 0.1265$  cm

Mean internal radius with 30% distension ( $r_{30}$ ):  $0.115 + 0.115(0.30) = 0.1495$  cm

Mean volume change for 10% distension ( $\Delta V_{10}$ ):  $(A_{10} - A_0) \cdot l = \pi[(r_{10})^2 - (r_0)^2] \cdot l = 8.72 \cdot 10^{-3}$  ml

## KNELLER ET AL.

Mean volume change for 30% distension ( $\Delta V_{30}$ ):  $(A_{30} - A_0) \cdot 1 = \pi[(r_{30})^2 - (r_0)^2] \cdot 1 = 2.87 \cdot 10^{-2}$  ml

Compliance for atherosclerotic vessel ( $C_A$ ):  $0.058 \cdot 10^{-3}$  ml/mm Hg

Compliance for normal vessel ( $C_N$ ):  $0.061 \cdot 10^{-3}$  ml/mm Hg

Pressure Range for Normal Vessels

Mean pressure change for 10% distension ( $\Delta P_{10N}$ ):  $\Delta V_{10}/C_N = 143$  mm Hg

Mean pressure change for 30% distension ( $\Delta P_{30N}$ ):  $\Delta V_{30}/C_N = 470$  mm Hg

Pressure Range for Atherosclerotic Vessels

Mean pressure change for 10% distension ( $\Delta P_{10A}$ ):  $\Delta V_{10}/C_A = 150$  mm Hg

Mean pressure change for 30% distension ( $\Delta P_{30A}$ ):  $\Delta V_{30}/C_A = 500$  mm Hg

Based on these calculations, pressures of 100, 300, and 500 mm Hg were examined in this study. The same pressure were applied for both normal and atherosclerotic vessels since the calculated pressures were similar.

## APPENDIX B

Calculation of Rabbit Iliac Artery Circumferential Dimension. The mean circumference of the rabbit iliac artery on the customized tissue stretching device (Figure 2a) corresponding to 10% and 30% distension can be calculated using  $r_{10}$  and  $r_{30}$  from Appendix A.

Mean circumference with 10% distension ( $Cir_{10}$ ):  $2 \cdot \pi \cdot r_{10} = 0.795$  cm

Mean circumference with 30% distension ( $Cir_{30}$ ):  $2 \cdot \pi \cdot r_{30} = 0.939$  cm

Received January 11, 1999; accepted May 25, 1999.